Interpreting Space-Based Trends in Carbon Monoxide with Multiple Models

Sarah A. Strode[1,2], Helen M. Worden[3], Megan Damon[2,4], Anne R. Douglass[2], Bryan N. Duncan[2], Louisa K. Emmons[3], Jean-Francois Lamarque[3], Michael Manyin[2,4], Luke D. Oman[2], Jose M. Rodriguez[2], Susan E. Strahan[1,2], Simone Tilmes[3]

[1]Universities Space Research Association, Columbia, MD, USA
[2]NASA Goddard Space Flight Center, Greenbelt, MD, USA
[3]National Center for Atmospheric Research, Boulder, CO, USA
[4]Science Systems and Applications, Inc., Lanham, MD, USA

Correspondence to: S. A. Strode (sarah.a.strode@nasa.gov)

Abstract

We use a series of chemical transport model and chemistry climate model simulations to investigate the observed negative trends in MOPITT CO over several regions of the world, and to examine the consistency of time-dependent emission inventories with observations. We find that simulations driven by the MACCity inventory, used for the Chemistry Climate Modeling Initiative (CCMI), reproduce the negative trends in the CO column observed by MOPITT for 2000-2010 over the eastern United States and Europe. However, the simulations have positive trends over eastern China, in contrast to the negative trends observed by MOPITT. The model bias in CO, after applying MOPITT averaging kernels, contributes to the model-observation discrepancy in the trend over eastern China. This demonstrates that biases in a model's average concentrations can influence the interpretation of the temporal trend compared to satellite observations. The total ozone column plays a role in determining the simulated tropospheric CO trends. A large positive anomaly in the simulated total ozone column in 2010 leads to a negative anomaly in OH and hence a positive anomaly in CO, contributing to the positive trend in simulated CO. These results demonstrate that accurately simulating variability in the ozone column is important for simulating and interpreting trends in CO.

1. Introduction

33   Carbon monoxide (CO) is an air pollutant that contributes to ozone formation and
34   affects the oxidizing capacity of the troposphere (Thompson, 1992; Crutzen, 1973).   Its
35   primary loss is through reaction with OH, which leads to a lifetime of 1-2 months (Bey et
36   al., 2001) and makes CO an excellent tracer of long-range transport.   Both fossil fuel
37   combustion and biomass burning are major sources of CO. The biomass burning source
38   shows large interannual variability (van der Werf et al., 2010), while fossil fuel emissions
39   typically change more gradually. The time-dependent MACCity inventory (Granier et
40   al., 2011) shows decreases in CO emissions from the United States and Europe from
41   2000 to 2010 due to increasing pollution controls, but increases in emissions from China.
42   MACCity emissions for years after 2000 are based on the Representative Concentration
43   Pathway (RCP) 8.5 (Riahi et al., 2007).   The REAS (Kurokawa et al., 2013) and
44   EDGAR4.2 (EC-JRC/PBL, 2011) inventories also show increasing CO emissions from
45   China. The bottom-up inventory of Zhang et al. (2009) shows an 18% increase in CO
46   emissions from China from 2001 to 2006, and Zhao et al. (2012) estimate a 6% increase
47   between 2005 and 2009.   However, there is considerable uncertainty in bottom-up
48   inventories, and comparison of model hindcast simulations driven by bottom-up
49   inventories with observations provides an important test of the time-dependent emission
50   estimates.

51   Space-based observations of CO are now available for over a decade and show
52   trends at both hemispheric and regional scales. Warner et al. (2013) found significant
53   negative trends in both background CO and recently emitted CO at 500 hPa over southern
54   hemisphere oceans and northern hemisphere land and ocean in Atmospheric Infrared
55   Sounder (AIRS) data. Worden et al. (2013) calculated trends in the CO column from
56   several thermal infrared (TIR) instruments including MOPITT and AIRS. They found
57   statistically significant negative trends over Europe, the eastern United States, and China
58   for 2002-2012. He et al. (2013) also report a negative trend in MOPITT near-surface CO
59   over western Maryland.

60   Surface concentrations of CO show downward trends over the United States
61   driven by emission reductions (EPA, 2011), consistent with the space-based trends.
62   Decreases in the partial column of CO from FTIR stations in Europe also show decreases
63   from 1996 to 2006, consistent with emissions decreases (Angelbratt et al., 2011). Yoon

and Pozzer (2014) found that a model simulation of 2001 to 2010 reproduced negative trends in surface CO over the eastern U.S. and western Europe, but showed a positive trend in surface CO over southern Asia.

The cause of the negative trend over China seen in MOPITT and AIRS data is uncertain. The trend is consistent with the results of Li and Liu (2011), who found decreases in surface CO measurements in Beijing, and with decreases in CO emissions in 2008 inferred from the correlation of CO with CO_2 measured at Hateruma Island (Tohjima et al., 2014) and at a rural site in China (Wang et al., 2010). Yumimoto et al. (2014) used inverse modeling of MOPITT data to infer a decrease in CO emissions from China after 2007. The 2008 Olympic Games and the 2009 global economic slowdown led to reductions in CO (Li and Liu, 2011; Worden et al., 2012). However, the negative trend in MOPITT CO is inconsistent with the rising CO emissions of the MACCity and REAS inventories. Inverse modeling of MOPITT version 6 data yields a negative trend in CO emissions from China and a larger global decline in CO emissions than that found in the MACCity inventory (Yin et al., 2015).

This study examines whether global hindcast simulations can reproduce the trends and variability in carbon monoxide seen in the MOPITT record. We examine the role of averaging kernels and the contribution of trends at different altitudes to the trends observed by MOPITT. We then examine the impact of OH variability on the simulated trends in CO.

2. Methods

2.1. MOPITT

The MOPITT instrument onboard the Terra Satellite provides the longest satellite-based record of atmospheric CO, with observations available from March 2000 to present. It provides nearly global coverage every three days (Edwards et al., 2004). We use the monthly Level 3 daytime column data from the Version 5 TIR product, which has negligible drift in the bias over time (Deeter et al., 2013). The level 3 data is a gridded product and includes the a priori and averaging kernel for each grid box. Supplemental Figure S1 shows the MOPITT column averaging kernels averaged over four regions. The column averaging kernels depend on the observed scene, and vary year to year as well as

94 seasonally. The dependence of the column averaging kernels on the CO mixing ratio
95 profile (Deeter, 2009) explains the high values in the lower troposphere over eastern
96 China in winter.

97   We calculate trends and de-seasonalized anomalies for the Eastern U.S., Europe, and
98 eastern China regions described by Worden et al. (2013). Trends that differ from zero by
99 more than the two-sigma uncertainty on the trend are considered statistically significant.
100 We account for autocorrelation of the data for a one-month lag when calculating the
101 uncertainty on the trends. We calculate the annual cycle by fitting the data with a series
102 of sines and cosines as well as the linear trend, and then remove the annual cycle to
103 obtain the de-seasonalized anomalies. Months with no MOPITT data or only a few days
104 of MOPITT data are excluded from the trend analysis. This includes May-August of
105 2001 and August-September of 2009. We report the MOPITT trends for 2000-2010 for
106 comparison with model simulations, and for 2000-2014 to give a longer-term view of the
107 observed trends.

108

109   **2.2. Model Simulations**
110   We use a suite of chemistry climate model (CCM) and chemical transport model
111 (CTM) simulations to interpret the observed trends. The Global Modeling Initiative
112 (GMI) CTM includes both tropospheric (Duncan et al., 2007) and stratospheric (Strahan
113 et al., 2007) chemistry, including over 400 reactions and 124 chemical species.
114 Meteorology for the GMI simulations comes from the Modern-Era Retrospective
115 Analysis for Research and Applications (MERRA) (Rienecker et al., 2011). The GEOS-
116 5 Chemistry Climate Model (GEOSCCM)(Oman et al., 2011) incorporates the GMI
117 chemical mechanism into the GEOS-5 atmospheric general circulation model (AGCM).
118 The GEOSCCM simulations are forced by observed sea surface temperatures (SSTs)
119 from (Reynolds et al., 2002).
120   The Community Earth System Model, CESM1 CAM4-chem, includes 191 chemical
121 tracers and over 400 reactions for both troposphere and stratosphere (Tilmes et al., 2016).
122 The model can be run fully coupled to a free-running ocean, with prescribed SSTs, or
123 with nudged meteorology from GEOS-5 or MERRA analysis. CESM1 CAM4-chem is

124 further coupled to the land model, providing biogenic emissions from the Model of
125 Emissions and Aerosols from Nature (MEGAN), version 2.1 (Guenther et al., 2012).

126   Several simulations were conducted as part of the Chemistry-Climate Model Initiative
127 (CCMI) project (Eyring et al., 2013). These include the Ref-C1 simulation of the
128 GEOSCCM and a Ref-C1 CESM1 CAM4-Chem simulation, hereafter called G-Ref-C1
129 and C-Ref-C1, respectively, and the Ref-C1-SD simulation of the GMI CTM. Both the
130 Ref-C1 and the Ref-C1-SD simulations use time-dependent anthropogenic and biomass
131 burning emissions from the MACCity inventory (Granier et al., 2011), but the Ref-C1-
132 SD simulations use specified meteorology while the Ref-C1 simulations run with
133 prescribed SSTs.   The MACCity inventory linearly interpolates the decadal
134 anthropogenic emissions from the ACCMIP inventory (Lamarque et al., 2010) for 2000,
135 and the RCP8.5 emissions for 2005 and 2010, to each year in between. The MACCity
136 biomass burning emissions have year-to-year variability based on the GFED-v2 (van der
137 Werf et al., 2006) inventory. From 2000 to 2010, CO emissions in the MACCity
138 inventory decreased from 31 to 11 Tg yr^{-1} over the eastern U.S., from 97 to 59 Tg yr^{-1}
139 over Europe, and increased from 56 Tg to 72 Tg yr^{-1} over eastern China.

140   Given the uncertainty in CO emissions, we conduct a GMI CTM simulation using an
141 alternative time-dependent emissions scenario, called AltEmis.   This simulation is
142 described in detail in (Strode et al., 2015b). Briefly, anthropogenic emissions include
143 time-dependence based on EPA (http://www.epa.gov/ttn/chief/trends/index.html), the
144 REAS   inventory   (Ohara   et   al.,   2007),   and   EMEP
145 (http://www.ceip.at/ms/ceip_home1/ceip_home/webdab_emepdatabase/reported_emissio
146 ndata/), and annual scalings from van Donkelaar et al. (2008). Biomass burning
147 emissions are based on the GFED3 inventory (van der Werf et al., 2010). While the
148 regional emission trends in this simulation are of the same sign as in the Ref-C1 case, the
149 magnitude of the negative trends over the U.S. and Europe are smaller and the positive
150 trend over China is larger, leading to a positive global trend (Fig. 1). We also conduct a
151 sensitivity study called EmFix with anthropogenic and biomass burning emissions held
152 constant at year 2000 levels. Table 1 summarizes the simulations used in this study.

153   We regrid the model output to the MOPITT grid and convolve the simulated CO with
154 the MOPITT averaging kernels and a priori in order to compare the simulated and

155 observed CO columns. The averaging kernels are space and time dependent. We use the

156 following equation from Deeter et al. (2013):

157      $C_{sim} = C_0 + \mathbf{a}(\mathbf{x}_{mod} - \mathbf{x}_0)$ (1)

158 where C_{sim} and C_0 are the simulated and a priori CO total columns, respectively, $\mathbf{a}$ is the

159 total column averaging kernel, and $\mathbf{x}_{mod}$ and $\mathbf{x}_0$ are the modeled and a priori CO profiles,

160 respectively. The column averaging kernel is calculated from the standard averaging

161 kernel matrix, which is based on the log of the CO concentration profile, following the

162 method of Deeter (2009):

163      $a_j = (K / \log_{10}e) \sum \Delta p_i \, v_{rtv,i} \, A_{ij}$ (2)

164 where Δp_i and $v_{rtv,i}$ are the pressure thickness and retrieved CO concentration,

165 respectively, of level i, $\mathbf{A}$ is the standard averaging kernel matrix, and $K = 2.12 * 10^{13}$

166 molec cm^{-2} hPa^{-1} ppb^{-1}.

167   We deseasonalize the simulated CO columns and calculate their linear trend

168 following the same procedure that we applied to the MOPITT CO. Months that do not

169 have MOPITT data (June-July 2001 and August-September 2009) are excluded from the

170 analysis of the model trends as well.

171 The Ref-C1 and Ref-C1-SD simulations requested by CCMI extend until 2010.

172 However, the MACCity biomass burning emissions extend only until 2008. CAM4-

173 Chem therefore repeated the biomass burning emissions for 2008 for years 2009-2010.

174 In contrast, the GEOSCCM Ref-C1 and GMI Ref-C1-SD simulations used emissions

175 from GFED3 (van der Werf et al., 2010) for years after 2008. Some simulations were

176 available through 2011, while others ended in 2010. We therefore report results for

177 2000-2010, but note that extending the analysis through 2011 does not alter the

178 conclusions.

179 **3. Results**

180 **3.1. Trends over Europe, the United States, and the Northern Hemisphere**

181 The hindcast simulations driven by MACCity emissions (G-Ref-C1, Ref-C1-SD, and

182 C-Ref-C1) show negative trends in CO over the U.S. and Europe that agree with the

183 observed slope from MOPITT within the uncertainty (Fig. 2, Table 2). The MOPITT

184   trends for both regions are statistically significant for both regions, as shown by Worden

185   et al. (2013). These results are consistent with the findings of Yin et al. (2015), whose

186   inversion of MOPITT data showed a posteriori trends in CO emissions over the U.S. and

187   western Europe that were consistent with but slightly larger than the a priori trends. The

188   EmFix hindcast shows a positive, though non-significant, trend for both regions,

189   indicating that the decrease in CO emissions is necessary for reproducing the downward

190   trend in the CO column. The AltEmis simulation fails to produce the negative trends,

191   despite including negative trends in regional emissions for both the U.S. and Europe.

192   The impact of these negative regional trends is insufficient to overcome the positive

193   global emission trend in the AltEmis scenario (Fig. 1), leading to positive trends in CO.

194   Figure 2 also reveals a negative bias in the simulated CO column between the models

195   and MOPITT. A low bias in simulated CO at northern latitudes is often present in global

196   models (Naik et al., 2013), and may indicate a high bias in northern hemisphere OH

197   (Strode et al., 2015a) or CO dry deposition (Stein et al., 2014), as well as an

198   underestimate of CO emissions.

199   The deseasonalized anomalies in the MOPITT and simulated CO columns are shown

200   in Fig. 2b,d, and the correlation coefficient between the observed and simulated monthly

201   anomalies are presented in Table 2b. The highest correlations are for the AltEmis and

202   Ref-C1-SD simulations of the GMI CTM. This result is consistent with the use of year-

203   specific meteorology, which we expect to better match the transport of particular years.

204   The lowest correlations are for the EmFix simulation. This is expected since the EmFix

205   simulation does not include inter-annual variability (IAV) in biomass burning. The IAV

206   in biomass burning makes a large contribution to the IAV of CO (Voulgarakis et al.,

207   2015).

208   The role of biomass burning in driving the CO variability is even more evident at the

209   hemispheric scale. Figure 2g,h shows the anomalies in MOPITT and the simulations for

210   the northern hemisphere (0-60N). The EmFix simulation shows almost no correlation,

211   while the other simulations have correlation coefficients exceeding 0.6 (Table 2).   The

212   role of changing anthropogenic emissions is also evident, as the Ref-C1-SD simulation

213   captures the 2008-2009 dip in the CO column while the EmFix simulation does not.

214   Gratz et al. (2015) found decreasing CO concentrations at Mount Bachelor Observatory

215 in Oregon during spring for 2004-2013, which they attribute to reductions in emissions
216 leading to a lower hemispheric background.   We also note that Ref-C1-SD and G-Ref-
217 C1 have similar correlations with the observed variability for the northern hemisphere
218 (Table 2), indicating that transport differences are less important for variability at the
219 hemispheric scale.

220 **3.2. Trend over China**

221 Observations from MOPITT show a negative trend in the CO column over eastern
222 China for 2002-2012 (Worden et al., 2013). The negative trend for the years 2000-2014
223 exceeds that for 2000-2010 (Table 2), showing that it is not driven solely by temporary
224 emission reductions in 2008. Our simulations do not reproduce this trend, and instead
225 show increases in the CO column (Fig. 2e), which is expected given that CO emissions
226 from China increase in four of the five simulations. The anomalies (Fig. 2f) show that
227 the discrepancy in the simulated versus observed trends is driven largely by the failure of
228 the simulations to capture the 2008 dip in the CO column, leading to an overestimate that
229 continues through 2010. This suggests emission reductions in China during this time
230 period are not adequately captured by the emission inventories. However, the good
231 agreement between the observed and simulated decreases in CO for the northern
232 hemisphere as a whole (Fig. 2g,h) suggest that on a global scale, the emission time series
233 is reasonable. Consequently, we examine several other factors that may contribute to the
234 difference in sign between the MOPITT and simulated CO trends.

235 Regional trends in CO are expected to vary with altitude, with surface concentrations
236 most heavily influenced by local emissions. MOPITT TIR retrievals have higher
237 sensitivity to CO in the mid-troposphere than at the surface (Deeter et al., 2004), so the
238 trend in the MOPITT CO column will be weighted towards the trends in free tropospheric
239 CO rather than near-surface CO. We quantify this impact on our Ref-C1-SD CO column
240 trends by comparing the trend in the pure-model CO column with that of the simulated
241 column convolved with the MOPITT averaging kernels.

242 The simulated CO trend over eastern China for 2000-2010 is positive (but not
243 significant) both with and without the averaging kernels, but application of the MOPITT
244 kernels increases the positive trend from $1.3*10^{16}$ molec cm^{-2} yr^{-1} to $1.4*10^{16}$ molec cm^{-2}
245 yr^{-1}. This result is initially surprising since we expect trends in the mid-troposphere to be

246   more strongly influenced by the decrease in the hemispheric CO background. Indeed, the

247   trends in CO concentration over eastern China simulated in Ref-C1-SD switch from

248   positive in the lower troposphere to negative in the middle and upper troposphere.

249   However, the application of the kernels results in more positive (or less negative) trends

250   in all regions.

251   Yoon et al. (2013) show that since the averaging kernels vary over time, a bias

252   between the true atmosphere and the a priori assumed by MOPITT can lead to an

253   artificial trend in the retrieved CO. Similarly, the bias between the average simulated CO

254   concentrations and the MOPITT a priori, evident in Figure 2, can lead to an artifact in the

255   simulated CO trend when the simulation is convolved with the MOPITT averaging

256   kernels. This is due to the changing contribution of the a priori when the vertical

257   sensitivity (averaging kernel) is varying in time. MOPITT vertical sensitivity varies with

258   time due to instrument degradation as well as the change in CO abundance.   The bias in

259   CO varies with altitude, so if the vertical sensitivity described by the averaging kernel

260   changes, this will change the value of the convolved CO column even if there were no

261   changes in the CO profile. Furthermore, changes in the averaging kernel result in more

262   or less weight placed on the a priori versus the CO simulated by the model. Thus, a

263   difference between the a priori and the model means that placing more (or less) weight on

264   the a priori will change the resulting value of C_{sim}. Since the a priori profiles and

265   columns are constant in time, taking the time derivative of equation 1 yields:

266       $\partial C_{sim}/\partial t = \mathbf{a}\ (\partial \mathbf{x}_{mod}/\partial t) + \partial \mathbf{a}/\partial t\ (\mathbf{x}_{mod} - \mathbf{x}_0)$ (3)

267   The second term on the right hand side shows that the larger the bias between the

268   modeled CO and the a priori, the larger the impact of the changing averaging kernel.

269   We quantify this effect by convolving the simulated CO for each year with the

270   MOPITT averaging kernels for the year 2008, thus removing the effect of the time-

271   dependence of the averaging kernels. The resulting trend, $0.56*10^{16}$ molec cm^{-2} yr^{-1}, is

272   less positive than the pure model trend or the original simulated trend. Thus, accounting

273   for the time-dependence of the averaging kernels convolved with model bias reduces but

274   does not eliminate the discrepancy with the observed trend. Other regions also show a

275   more negative trend when the same averaging kernel is applied to the model results for

276   all years. The large bias in CO at middle and high northern latitudes commonly seen in

277 modeling studies thus impacts the ability of models to reproduce and attribute observed
278 trends in satellite data.

279   Figure 2 and Table 2 also show a positive trend in the GMI EmFix simulation for
280 eastern China. This larger trend in the EmFix simulation than the Ref-C1-SD simulation
281 indicates that the net decrease in emissions contributes to decreasing CO over eastern
282 China, consistent with the observed negative trend, but other factors in the model cause
283 an increase in CO over eastern China even when all emissions are constant. The trend in
284 the EmFix simulation thus contributes to the erroneous sign of the trend in the GMI
285 simulations. The trends in the EmFix simulation for the northern hemisphere average and
286 the eastern U.S. and Europe are positive as well (Table 2). We examine their cause in the
287 next section.

288   **3.3. Contribution of OH Interannual Variability**

289

290   Since the EmFix simulation shows a positive trend in the northern hemisphere, we
291 next examine the variability in the CO sink, OH. We also examine variability in the total
292 ozone column, since overhead ozone is a major driver of OH variability (Duncan and
293 Logan, 2008). Figure 3 shows the variability in CO and OH in the EmFix simulation.
294 The positive and negative anomalies in CO correspond with the negative and positive
295 anomalies, respectively, in OH. The anomalies in OH are in turn inversely related to
296 anomalies in the total ozone column. The correlation coefficient between OH and
297 column ozone is -0.53 for the 15°S-15°N average, -0.72 for the 15°-25°N average, and -
298 0.75 for the 30°-60°N average. The large NH ozone anomaly in 2010, in particular, leads
299 to a large anomaly in OH and thus CO. This OH anomaly extends from the northern
300 tropics to the midlatitudes. The large CO anomaly near the end of the time series
301 contributes to the apparent 11-year trend. We note that since the lifetime of CO is several
302 months, CO anomalies are not expected to have a one-to-one correspondence with the
303 OH anomalies.
304   The large anomaly in the simulated total ozone column in 2010 is overestimated
305 compared to observations. Figure 4 shows the time-dependence of the total ozone
306 column from 30°-60°N in EmFix compared to SBUV data (Frith et al., 2014). While the
307 observations show an anomaly in 2010, the magnitude is smaller than that produced by

308   the simulation. Steinbrecht et al. (2011) attribute the 2010 anomaly in northern

309   midlatitude ozone observations to a combination of an unusually strong negative Arctic

310   Oscillation and North Atlantic Oscillation and the easterly phase of the quasi-biennial

311   oscillation.

312   While the impact of OH interannual variability on the apparent trend in CO is clear in

313   the EmFix simulation, this source of variability is partially masked by large interannual

314   variability in CO emissions in the other simulations. We examine the correlation

315   between the de-trended and deseasonalized CO anomalies from 10°S-10°N in the Ref-

316   C1-SD simulation and the CO emissions as well as the simulated OH and column ozone.

317   Since the CO emitted in a given month can influence concentrations for several

318   subsequent months, we use a 3-month smoothing of the emission time series. We find a

319   high correlation (r=0.88) between the CO anomalies and the CO emissions. This

320   correlation is also evident in the MOPITT data, as the MOPITT CO anomalies have a

321   correlation of r=0.70 with the emissions. Figure 5 shows the strong relationship between

322   the simulated CO anomalies and the CO emissions. However, the colors in Fig. 5

323   indicate that the scatter for a given level of emissions is often linked to the OH

324   anomalies, with low/high OH anomalies leading to CO that is higher/lower than would be

325   predicted just from the CO emissions. We find that the 10°S-10°N OH in the Ref-C1-SD

326   simulation is anticorrelated with CO (r=-0.62) and with the total ozone column (r=-0.68).

327   Consequently, the simulated ozone column plays a role in modulating tropical CO

328   variability even when variable CO emissions are included, although the emissions still

329   play the strongest role.

330 **4. Conclusions**

331   We conducted a series of multi-year simulations to analyze the causes of the negative

332   trends in MOPITT CO reported by Worden et al. (2013). Both CTM and CCM

333   simulations driven by the MACCity emissions reproduce the observed trends over the

334   eastern U.S. and Europe, providing confidence in the regional emission trends.

335   None of the simulations reproduce the observed negative trend over eastern China.

336   This negative trend persists even with the MOPITT data extended out to 2014. The

337   MOPITT averaging kernels are weighted towards the free troposphere, where the relative

338 importance of hemispheric versus local trends is greater. However, our simulations
339 indicate that this effect is insufficient to explain the negative trends over China. While
340 this likely indicates a too positive emission trend for China, several other factors play a
341 role in the model-observation mismatch. We find that the time-dependent MOPITT
342 averaging kernels, combined with the low bias in simulated CO, provides a positive
343 component to the simulated trends. Large anomalies in the simulated ozone column in
344 the GMI CTM simulations also contribute a positive component to the northern
345 hemisphere trends due to their impact on OH.

346 Variability in emissions is the primary driver of year-to-year variability in simulated
347 CO, but OH variability also plays a role. The simulated OH is anti-correlated with both
348 CO and the total ozone column, highlighting the importance of realistic overhead ozone
349 columns for accurately simulating CO variability and trends. In addition, further work is
350 needed to understand recent changes in CO emissions from China.

351

352 **Acknowledgements**

353 This work was supported by NASA's Modeling, Analysis, and Prediction program
354 and computing resources from the NASA High-End Computing Program. We thank
355 Bruce Van Aartsen for contributing to the GMI simulations. The CESM project is
356 supported by the National Science Foundation and the Office of Science (BER) of the US
357 Department of Energy. The MOPITT project is supported by the NASA Earth Observing
358 System (EOS) Program. The National Center for Atmospheric Research (NCAR) is
359 sponsored by the National Science Foundation.

360

361
362 Angelbratt, J., Mellqvist, J., Simpson, D., Jonson, J., Blumenstock, T., Borsdorff, T.,
363 Duchatelet, P., Forster, F., Hase, F., Mahieu, E., De Maziere, M., Notholt, J., Petersen,
364 A., Raffalski, U., Servais, C., Sussmann, R., Warneke, T., and Vigouroux, C.: Carbon
365 monoxide (CO) and ethane (C2H6) trends from ground-based solar FTIR measurements
366 at six European stations, comparison and sensitivity analysis with the EMEP model,
367 Atmospheric Chemistry and Physics, 11, 9253-9269, 10.5194/acp-11-9253-2011, 2011.
368 Bey, I., Jacob, D., Logan, J., and Yantosca, R.: Asian chemical outflow to the Pacific in
369 spring: Origins, pathways, and budgets, Journal of Geophysical Research-Atmospheres,
370 106, 23097-23113, 10.1029/2001JD000806, 2001.

371 Crutzen, P.: A Discussion of the Chemistry of Some Minor Constituents in the
372 Stratosphere and Troposphere, Pure and Applied Geophysics, 106, 1385-1399,
373 10.1007/BF00881092, 1973.
374 Deeter, M., Emmons, L., Edwards, D., Gille, J., and Drummond, J.: Vertical resolution
375 and information content of CO profiles retrieved by MOPITT, Geophysical Research
376 Letters, 31, 10.1029/2004GL020235, 2004.
377 Deeter, M. N.: MOPITT (Measurements of Pollution in the Troposphere) Validated
378 Version 4 Product User's Guide, National Center for Atmospheric Research. Available
379 at http://web3.acd.ucar.edu/mopitt/v4_users_guide_val.pdf, 2009.
380 Deeter, M. N., Martinez-Alonso, S., Edwards, D. P., Emmons, L. K., Gille, J. C.,
381 Worden, H. M., Pittman, J. V., Daube, B. C., and Wofsy, S. C.: Validation of MOPITT
382 Version 5 thermal-infrared, near-infrared, and multispectral carbon monoxide profile
383 retrievals for 2000-2011, Journal of Geophysical Research-Atmospheres, 118, 6710-
384 6725, 10.1002/jgrd.50272, 2013.
385 Duncan, B. N., Strahan, S. E., Yoshida, Y., Steenrod, S. D., and Livesey, N.: Model study
386 of the cross-tropopause transport of biomass burning pollution, Atmospheric Chemistry
387 and Physics, 7, 3713-3736, 2007.
388 Duncan, B. N., and Logan, J. A.: Model analysis of the factors regulating the trends and
389 variability of carbon monoxide between 1988 and 1997, Atmospheric Chemistry and
390 Physics, 8, 7389-7403, 2008.
391 Edwards, D. P., Emmons, L. K., Hauglustaine, D. A., Chu, D. A., Gille, J. C., Kaufman,
392 Y. J., Petron, G., Yurganov, L. N., Giglio, L., Deeter, M. N., Yudin, V., Ziskin, D. C.,
393 Warner, J., Lamarque, J. F., Francis, G. L., Ho, S. P., Mao, D., Chen, J., Grechko, E. I.,
394 and Drummond, J. R.: Observations of carbon monoxide and aerosols from the Terra
395 satellite: Northern Hemisphere variability, Journal of Geophysical Research-
396 Atmospheres, 109, 10.1029/2004jd004727, 2004.
397 EPA: Our Nation's Air - Status and Trends through 2010, edited by: EPA-454/R-12-001,
398 Research Triangle Park, NC, 2011.
399 Eyring, V., Lamarque, J.-F., Hess, P., Arfeuille, F., Bowman, K., Chipperfiel, M. P.,
400 Duncan, B., Fiore, A., Gettelman, A., and Giorgetta, M. A.: Overview of IGAC/SPARC
401 Chemistry-Climate Model Initiative (CCMI) community simulations in support of
402 upcoming ozone and climate assessments, Sparc Newsletter, 40, 48-66, 2013.
403 Frith, S., Kramarova, N., Stolarski, R., McPeters, R., Bhartia, P., and Labow, G.: Recent
404 changes in total column ozone based on the SBUV Version 8.6 Merged Ozone Data Set,
405 Journal of Geophysical Research: Atmospheres, 119, 9735-9751, 2014.
406 Granier, C., Bessagnet, B., Bond, T., D'Angiola, A., van der Gon, H. D., Frost, G. J.,
407 Heil, A., Kaiser, J. W., Kinne, S., Klimont, Z., Kloster, S., Lamarque, J. F., Liousse, C.,
408 Masui, T., Meleux, F., Mieville, A., Ohara, T., Raut, J. C., Riahi, K., Schultz, M. G.,
409 Smith, S. J., Thompson, A., van Aardenne, J., van der Werf, G. R., and van Vuuren, D.
410 P.: Evolution of anthropogenic and biomass burning emissions of air pollutants at global
411 and regional scales during the 1980-2010 period, Climatic Change, 109, 163-190,
412 10.1007/s10584-011-0154-1, 2011.
413 Gratz, L., Jaffe, D., and Hee, J.: Causes of increasing ozone and decreasing carbon
414 monoxide in springtime at the Mt. Bachelor Observatory from 2004 to 2013,
415 Atmospheric Environment, 109, 323-330, 10.1016/j.atmosenv.2014.05.076, 2015.

416 Guenther, A., Jiang, X., Heald, C., Sakulyanontvittaya, T., Duhl, T., Emmons, L., and
417 Wang, X.: The Model of Emissions of Gases and Aerosols from Nature version 2.1
418 (MEGAN2. 1): an extended and updated framework for modeling biogenic emissions,
419 2012.
420 He, H., Stehr, J., Hains, J., Krask, D., Doddridge, B., Vinnikov, K., Canty, T., Hosley, K.,
421 Salawitch, R., and Worden, H.: Trends in emissions and concentrations of air pollutants
422 in the lower troposphere in the Baltimore/Washington airshed from 1997 to 2011,
423 Atmospheric Chemistry and Physics, 13, 7859-7874, 2013.
424 Kurokawa, J., Ohara, T., Morikawa, T., Hanayama, S., Janssens-Maenhout, G., Fukui, T.,
425 Kawashima, K., and Akimoto, H.: Emissions of air pollutants and greenhouse gases over
426 Asian regions during 2000-2008: Regional Emission inventory in ASia (REAS) version
427 2, Atmospheric Chemistry and Physics, 13, 11019-11058, 10.5194/acp-13-11019-2013,
428 2013.
429 Lamarque, J.F., Bond, T.C., Eyring, V., Granier, C., Heil, A., Klimont, Z., Lee, D.,
430 Liousse, C., Mieville, A., Owen, B. and Schultz, M.G.: Historical (1850–2000) gridded
431 anthropogenic and biomass burning emissions of reactive gases and aerosols:
432 methodology and application, Atmospheric Chemistry and Physics, 10, 7017-7039, 2010.
433 Li, L., and Liu, Y.: Space-borne and ground observations of the characteristics of CO
434 pollution in Beijing, 2000–2010, Atmospheric Environment, 45, 2367-2372,
435 http://dx.doi.org/10.1016/j.atmosenv.2011.02.026, 2011.
436 Naik, V., Voulgarakis, A., Fiore, A. M., Horowitz, L. W., Lamarque, J. F., Lin, M.,
437 Prather, M. J., Young, P. J., Bergmann, D., Cameron-Smith, P. J., Cionni, I., Collins, W.
438 J., Dalsoren, S. B., Doherty, R., Eyring, V., Faluvegi, G., Folberth, G. A., Josse, B., Lee,
439 Y. H., MacKenzie, I. A., Nagashima, T., van Noije, T. P. C., Plummer, D. A., Righi, M.,
440 Rumbold, S. T., Skeie, R., Shindell, D. T., Stevenson, D. S., Strode, S., Sudo, K., Szopa,
441 S., and Zeng, G.: Preindustrial to present-day changes in tropospheric hydroxyl radical
442 and methane lifetime from the Atmospheric Chemistry and Climate Model
443 Intercomparison Project (ACCMIP), Atmospheric Chemistry and Physics, 13, 5277-
444 5298, 10.5194/acp-13-5277-2013, 2013.
445 Ohara, T., Akimoto, H., Kurokawa, J., Horii, N., Yamaji, K., Yan, X., and Hayasaka, T.:
446 An Asian emission inventory of anthropogenic emission sources for the period 1980-
447 2020, Atmospheric Chemistry and Physics, 7, 4419-4444, 2007.
448 Oman, L. D., Ziemke, J. R., Douglass, A. R., Waugh, D. W., Lang, C., Rodriguez, J. M.,
449 and Nielsen, J. E.: The response of tropical tropospheric ozone to ENSO, Geophysical
450 Research Letters, 38, 10.1029/2011gl047865, 2011.
451 Reynolds, R., Rayner, N., Smith, T., Stokes, D., and Wang, W.: An improved in situ and
452 satellite SST analysis for climate, Journal of Climate, 15, 1609-1625, 10.1175/1520-
453 0442(2002)015<1609:AIISAS>2.0.CO;2, 2002.
454 Riahi, K., Grübler, A., and Nakicenovic, N.: Scenarios of long-term socio-economic and
455 environmental development under climate stabilization, Technological Forecasting and
456 Social Change, 74, 887-935, 2007.
457 Rienecker, M. M., Suarez, M. J., Gelaro, R., Todling, R., Bacmeister, J., Liu, E.,
458 Bosilovich, M. G., Schubert, S. D., Takacs, L., Kim, G.-K., Bloom, S., Chen, J., Collins,
459 D., Conaty, A., da Silva, A., Gu, W., Joiner, J., Koster, R. D., Lucchesi, R., Molod, A.,
460 Owens, T., Pawson, S., Pegion, P., Redder, C. R., Reichle, R., Robertson, F. R., Ruddick,
461 A. G., Sienkiewicz, M., and Woollen, J.: MERRA: NASA's Modern-Era Retrospective

Analysis for Research and Applications, Journal of Climate, 24, 3624-3648, 10.1175/JCLI-D-11-00015.1, 2011.

Stein, O., Schultz, M., Bouarar, I., Clark, H., Huijnen, V., Gaudel, A., George, M., and Clerbaux, C.: On the wintertime low bias of Northern Hemisphere carbon monoxide found in global model simulations, Atmospheric Chemistry and Physics, 14, 9295-9316, 10.5194/acp-14-9295-2014, 2014.

Steinbrecht, W., Köhler, U., Claude, H., Weber, M., Burrows, J.P., and van der A, R.J.: Very high ozone columns at northern mid-latitudes in 2010, Geophysical Research Letters, 38, 10.1029/2010GL046634, 2011.

Strahan, S. E., Duncan, B. N., and Hoor, P.: Observationally derived transport diagnostics for the lowermost stratosphere and their application to the GMI chemistry and transport model, Atmospheric Chemistry and Physics, 7, 2435-2445, 2007.

Strode, S., Duncan, B., Yegorova, E., Kouatchou, J., Ziemke, J., and Douglass, A.: Implications of carbon monoxide bias for methane lifetime and atmospheric composition in chemistry climate models, Atmospheric Chemistry and Physics, 15, 11789-11805, 2015a.

Strode, S. A., Rodriguez, J. M., Logan, J. A., Cooper, O. R., Witte, J. C., Lamsal, L. N., Damon, M., Van Aartsen, B., Steenrod, S. D., and Strahan, S. E.: Trends and variability in surface ozone over the United States, Journal of Geophysical Research: Atmospheres, 120, 9020-9042, 2015b.

Thompson, A.: The Oxidizing Capacity of the Earth's Atmosphere: Probable Past and Future Change, Science, 256, 1157-1165, 10.1126/science.256.5060.1157, 1992.

Tilmes, S., Lamarque, J. F., Emmons, L. K., Kinnison, D. E., Marsh, D., Garcia, R. R., Smith, A. K., Neely, R. R., Conley, A., Vitt, F., Val Martin, M., Tanimoto, H., Simpson, I., Blake, D. R., and Blake, N.: Representation of the Community Earth System Model (CESM1) CAM4-chem within the Chemistry-ClimateModel Initiative (CCMI), Geosci. Model Dev. Discuss., 2016, 1-50, 10.5194/gmd-2015-237, 2016.

Tohjima, Y., Kubo, M., Minejima, C., Mukai, H., Tanimoto, H., Ganshin, A., Maksyutov, S., Katsumata, K., Machida, T., and Kita, K.: Temporal changes in the emissions of CH_4 and CO from China estimated from CH_4/CO_2 and CO/CO_2 correlations observed at Hateruma Island, Atmospheric Chemistry and Physics, 14, 1663-1677, 10.5194/acp-14-1663-2014, 2014.

van der Werf, G. R., Randerson, J. T., Giglio, L., Collatz, G. J., Kasibhatla, P.S., and Arellano, Jr., A.F.: Interannual variability in global biomass burning emissions from 1997-2004, Atmospheric Chemistry and Physics, 6, 3423-3441, 2006.

van der Werf, G. R., Randerson, J. T., Giglio, L., Collatz, G. J., Mu, M., Kasibhatla, P. S., Morton, D. C., DeFries, R. S., Jin, Y., and van Leeuwen, T. T.: Global fire emissions and the contribution of deforestation, savanna, forest, agricultural, and peat fires (1997-2009), Atmospheric Chemistry and Physics, 10, 11707-11735, 10.5194/acp-10-11707-2010, 2010.

van Donkelaar, A., Martin, R. V., Leaitch, W. R., Macdonald, A. M., Walker, T. W., Streets, D. G., Zhang, Q., Dunlea, E. J., Jimenez, J. L., Dibb, J. E., Huey, L. G., Weber, R., and Andreae, M. O.: Analysis of aircraft and satellite measurements from the Intercontinental Chemical Transport Experiment (INTEX-B) to quantify long-range transport of East Asian sulfur to Canada, Atmospheric Chemistry and Physics, 8, 2999-3014, 2008.

508   Voulgarakis, A., Marlier, M., Faluvegi, G., Shindell, D., Tsigaridis, K., and Mangeon, S.:
509   Interannual variability of tropospheric trace gases and aerosols: The role of biomass
510   burning emissions, Journal of Geophysical Research-Atmospheres, 120, 7157-7173,
511   10.1002/2014JD022926, 2015.
512   Wang, Y., Munger, J., Xu, S., McElroy, M., Hao, J., Nielsen, C., and Ma, H.: CO2 and its
513   correlation with CO at a rural site near Beijing: implications for combustion efficiency in
514   China, Atmospheric Chemistry and Physics, 10, 8881-8897, 10.5194/acp-10-8881-2010,
515   2010.
516   Warner, J., Carminati, F., Wei, Z., Lahoz, W., and Attie, J.: Tropospheric carbon
517   monoxide variability from AIRS under clear and cloudy conditions, Atmospheric
518   Chemistry and Physics, 13, 12469-12479, 10.5194/acp-13-12469-2013, 2013.
519   Worden, H. M., Cheng, Y., Pfister, G., Carmichael, G. R., Zhang, Q., Streets, D. G.,
520   Deeter, M., Edwards, D. P., Gille, J. C., and Worden, J. R.: Satellite-based estimates of
521   reduced CO and CO2 emissions due to traffic restrictions during the 2008 Beijing
522   Olympics, Geophysical Research Letters, 39, 2012.
523   Worden, H. M., Deeter, M. N., Frankenberg, C., George, M., Nichitiu, F., Worden, J.,
524   Aben, I., Bowman, K. W., Clerbaux, C., Coheur, P. F., de Laat, A. T. J., Detweiler, R.,
525   Drummond, J. R., Edwards, D. P., Gille, J. C., Hurtmans, D., Luo, M., Martinez-Alonso,
526   S., Massie, S., Pfister, G., and Warner, J. X.: Decadal record of satellite carbon monoxide
527   observations, Atmospheric Chemistry and Physics, 13, 837-850, 10.5194/acp-13-837-
528   2013, 2013.
529   Yin, Y., Chevallier, F., Ciais, P., Broquet, G., Fortems-Cheiney, A., Pison, I., and
530   Saunois, M.: Decadal trends in global CO emissions as seen by MOPITT, Atmos. Chem.
531   Phys., 15, 13433-13451, 10.5194/acp-15-13433-2015, 2015.
532   Yoon, J., Pozzer, A., Hoor, P., Chang, D., Beirle, S., Wagner, T., Schloegl, S., Lelieveld,
533   J., and Worden, H.: Technical Note: Temporal change in averaging kernels as a source of
534   uncertainty in trend estimates of carbon monoxide retrieved from MOPITT, Atmospheric
535   Chemistry and Physics, 13, 11307-11316, 10.5194/acp-13-11307-2013, 2013.
536   Yoon, J., and Pozzer, A.: Model-simulated trend of surface carbon monoxide for the
537   2001-2010 decade, Atmospheric Chemistry and Physics, 14, 10465-10482, 10.5194/acp-
538   14-10465-2014, 2014.
539   Yumimoto, K., Uno, I., and Itahashi, S.: Long-term inverse modeling of Chinese CO
540   emission from satellite observations, Environmental Pollution, 195, 308-318,
541   10.1016/j.envpol.2014.07.026, 2014.
542   Zhang, Q., Streets, D. G., Carmichael, G. R., He, K. B., Huo, H., Kannari, A., Klimont,
543   Z., Park, I. S., Reddy, S., Fu, J. S., Chen, D., Duan, L., Lei, Y., Wang, L. T., and Yao, Z.
544   L.: Asian emissions in 2006 for the NASA INTEX-B mission, Atmospheric Chemistry
545   and Physics, 9, 5131-5153, 2009.
546   Zhao, Y., Nielsen, C. P., McElroy, M. B., Zhang, L., and Zhang, J.: CO emissions in
547   China: Uncertainties and implications of improved energy efficiency and emission
548   control, Atmospheric Environment, 49, 103-113, 10.1016/j.atmosenv.2011.12.015, 2012.
549

550

Table 1: Description of Simulations

Simulation	Model	Meteorology	Anthropogenic Emissions	Biomass Burning Emissions
G-Ref-C1	GEOSCCM	internally derived	MACCity	MACCity, GFED3 (2009-2010)
C-Ref-C1	CAM4-Chem	internally derived	MACCity	MACCity, then repeat 2008
Ref-C1-SD	GMI	MERRA	MACCity	Same as GEOSCCM
EmFix	GMI	MERRA	Fixed at 2000	Fixed at 2000
AltEmis	GMI	MERRA	Strode et al [2015]	GFED3

Table 2: Regional Trends and Correlations

a. Trends[1,2]

	Years	E. USA	Europe	E. China	N. Hemisphere
G-Ref-C1[3]	2000-2010	-2.2 (0.38)	-1.8 (0.42)	2.2 (1.1)	-0.76 (3.0)
C-Ref-C1[3]	2000-2010	-3.4 (0.54)	-2.9 (0.50)	1.4 (1.4)	-0.90 (3.0)
Ref-C1-SD[3]	2000-2010	-2.4 (0.53)	-1.6 (0.59)	1.4 (1.1)	-0.76 (3.0)
EmFix[3]	2000-2010	1.3 (0.55)	1.5 (0.44)	2.1 (0.87)	0.96 (2.5)
AltEmis[3]	2000-2010	0.71 (0.73)	0.74 (0.66)	3.8 (1.4)	1.1 (3.4)
MOPITT	*2000-2010*	*-2.5 (0.64)*	*-1.8 (0.69)*	*-2.9 (1.8)*	*-1.4 (2.8)*
MOPITT	*2000-2014*	*-2.1 (0.41)*	*-1.7 (0.43)*	*-3.1 (1.1)*	*-1.4 (1.7)*

[1]10^{16} molec cm^{-2} yr^{-1}

[2]1-sigma uncertainty given in parentheses

[3]Simulation results convolved with MOPITT averaging kernel and a priori

b. Correlation coefficient (r) with monthly MOPITT anomalies[1,2]

	Years	E. USA	Europe	E. China	N. Hemisphere
G-Ref-C1	2000-2010	**0.26**	**0.39**	0.061	**0.71**
C-Ref-C1	2000-2010	0.23	**0.36**	0.18	**0.62**
Ref-C1-SD	2000-2010	**0.43**	**0.51**	**0.39**	**0.73**
EmFix	2000-2010	0.10	0.21	0.071	0.059
AltEmis	2000-2010	**0.55**	**0.59**	**0.48**	**0.69**

[1]Correlations are calculated from the de-trended and de-seasonalized time series.

[2]Statistically significant correlations at the 95% confidence level are indicated in bold.
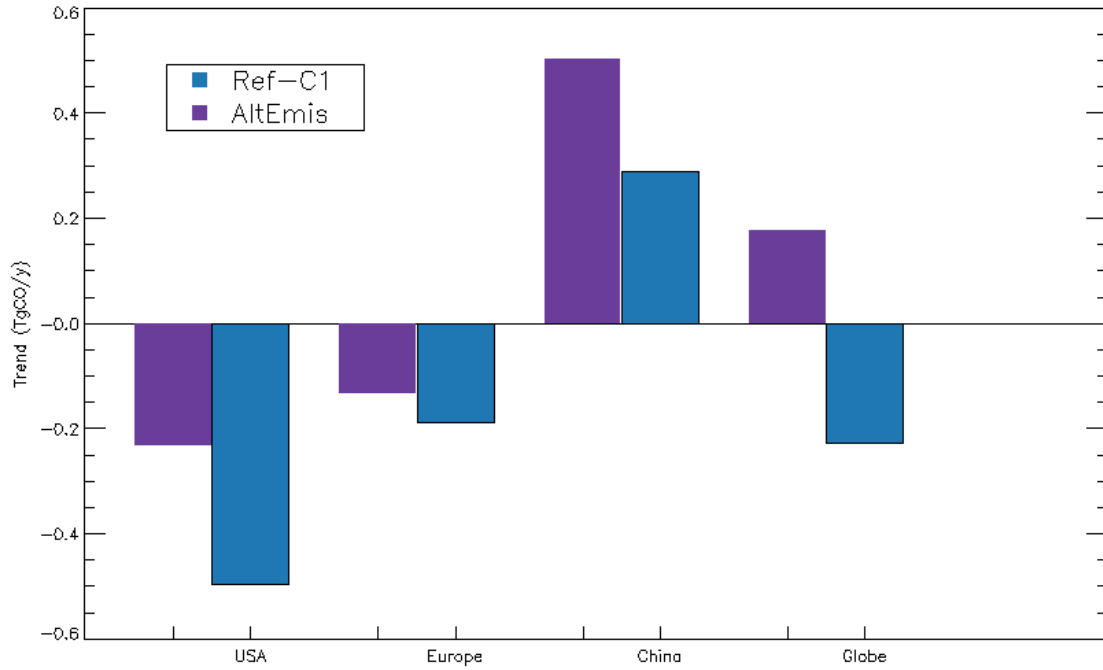
Figure 1: Trends in the CO emissions used in the Ref-C1 and Ref-C1-SD simulations (blue bars) and AltEmis simulation (purple bars) over 2000-2010 for the United States, Europe, China, and the world.
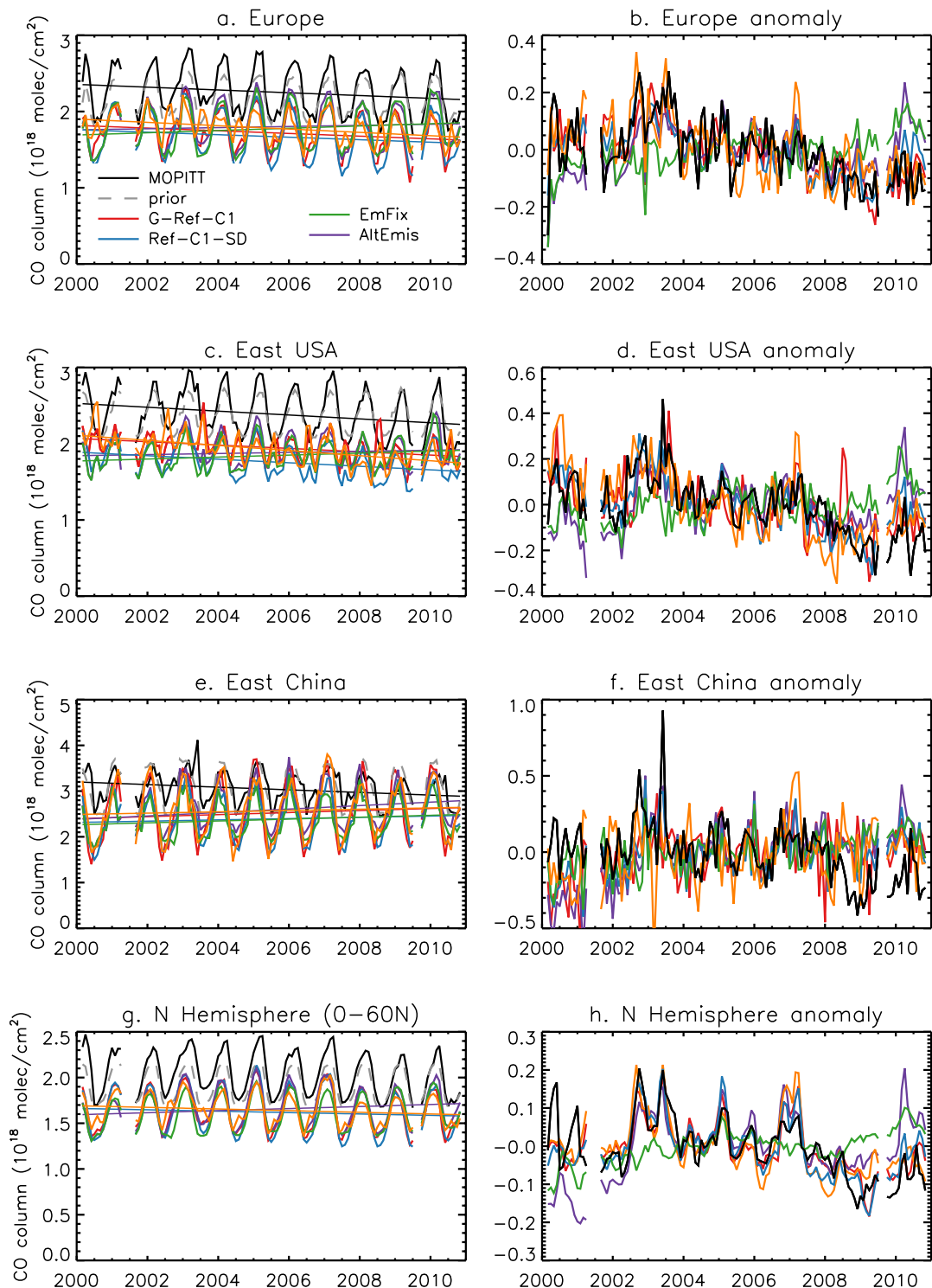
Figure 2: The time series and trends (left column) and de-seasonalized monthly anomalies (right column) of the CO column from MOPITT (black), the MOPITT a priori (gray), and simulated by G-Ref-C1 (red), Ref-C1-SD (blue), EmFix (green), C-Ref-C1 (orange), and AltEmis (purple) for 2000-2010. The regions shown are (a,b) Europe (0°-

15°E, 45°-55°N), (c,d) eastern U.S.A. (95°-75°W, 35°-40°N), (e,f) eastern China (110°-123°E, 30°-40°N), and (g,h) the northern hemisphere (0°-60°N).
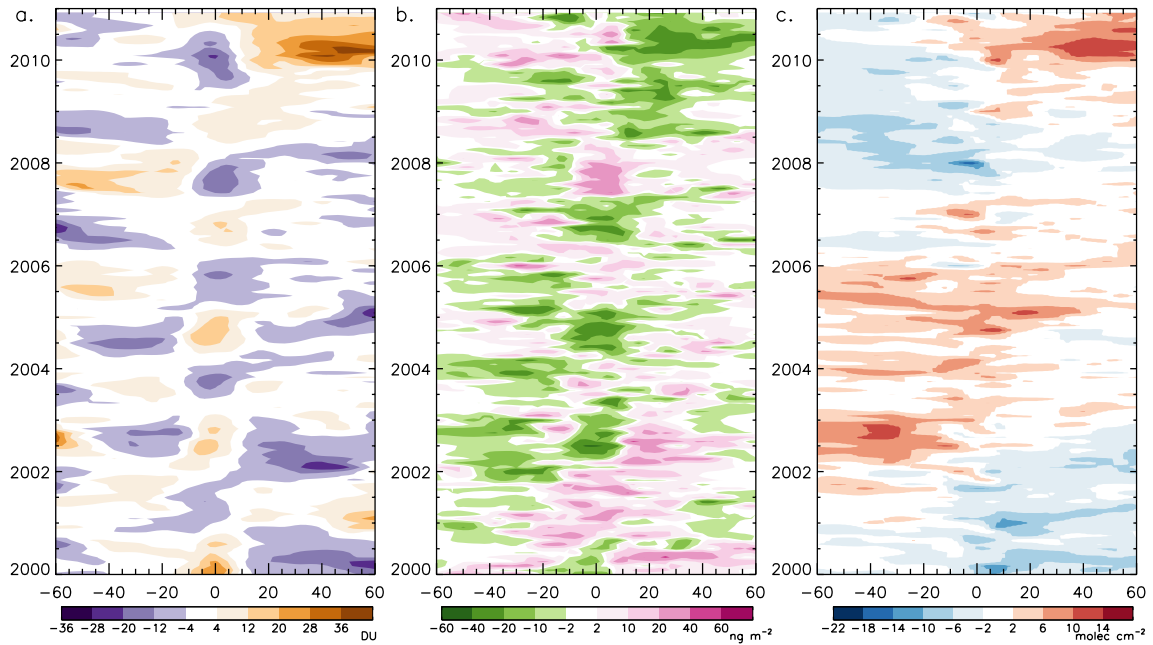
Figure 3: Deseasonalized monthly anomalies in the total ozone column (left), mean tropospheric OH (center), and CO column (right) from the EmFix simulation as a function of latitude and month.
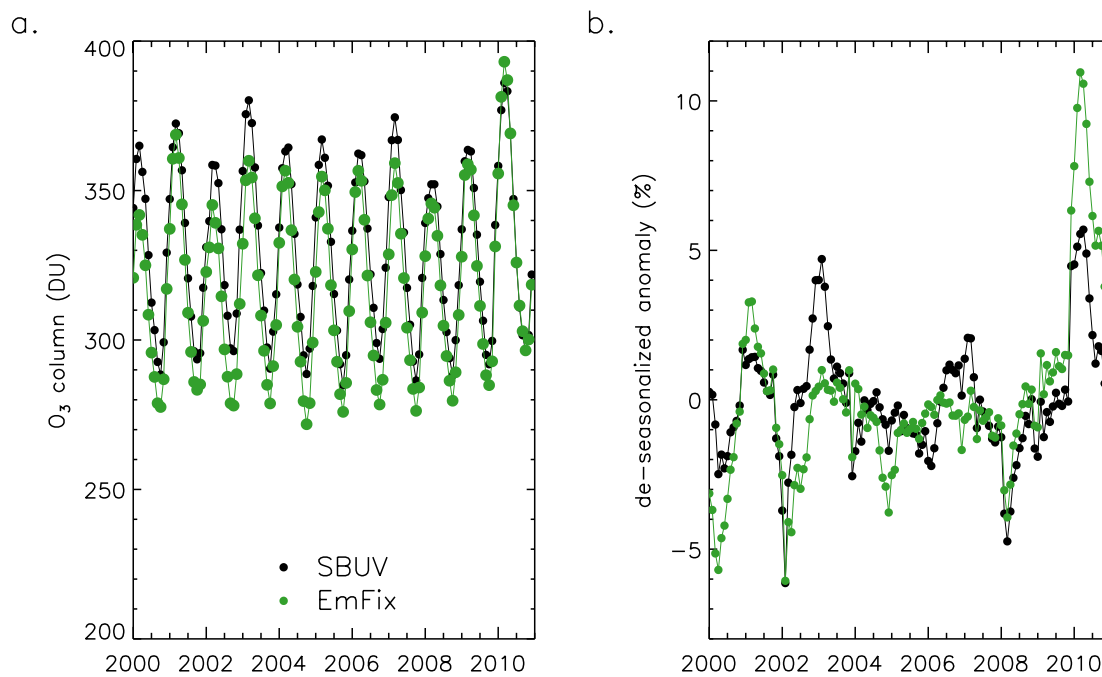
Figure 4: Monthly ozone column (a) and de-seasonalized ozone column anomaly (b) in SBUV data (black) and the EmFix simulation (green) for 30°-60°N.
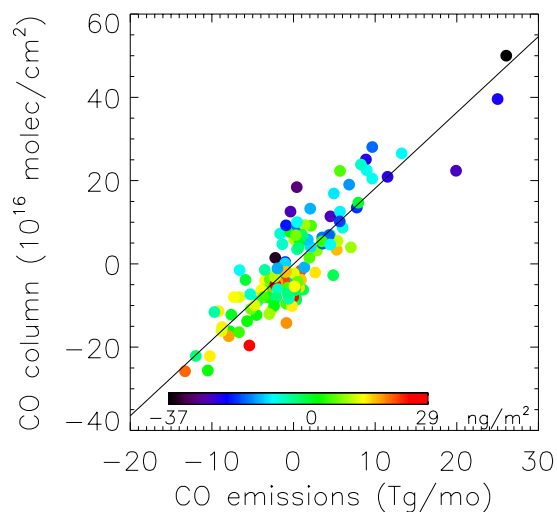
Figure 5: Monthly simulated CO column anomalies from the Ref-C1-SD simulation as a function of CO emissions for 10°S-10°N. Colors indicate the simulated OH column anomaly for the given month.